Optimization of Mold Flux for the Continuous Casting of Cr-Contained Steels

WANLIN WANG, JIE YU, LEJUN ZHOU, ZHAOYANG WU, and HUAN LI

To compensate the negative effect caused by the absorption of chromium oxide inclusions during the casting process of Cr-contained steels, a new mold flux system has been designed and investigated. The melting temperature range of the newly designed mold flux system is from [1124 K to 1395 K (851 °C to 1122 °C)]. The viscosity at 1573 K (1300 °C) and the break temperature increase with the addition of MnO and Cr_2O_3 but decrease with the addition of B_2O_3. The crystalline fraction of mold flux decreases from 81 to 42.1 pct with the addition of MnO and Cr_2O_3, and then further decreases to 25.3 pct with the addition of B_2O_3; however, it improves from 54.4 to 81.5 pct when the basicity increases. Besides, the heat-transfer ability of mold flux is inverse to the crystallization ratio of the slag. The comprehensive study of the properties for the four designed mold fluxes suggests that the mold flux with 1.15 basicity-3.01 pct B_2O_3-1.10 pct MnO-2.10 pct Cr_2O_3 shows the best properties for the continuous casting of Cr-contained steels.

I. INTRODUCTION

MOLD flux has been widely used in the continuous casting process, which can absorb inclusions and insulate molten steel from oxidation when it floats on the top of the molten steel. It also tends to lubricate the strand and moderate the horizontal heat transfer in the mold when it infiltrates into the gap between the mold wall and solidified shell.

During the metallurgical process of Cr-contained steels, such as Cr12MoV, the alloy element Cr in molten steel is easy to be oxidized during the smelting, refining, and continuous casting processes, as it has a closer affinity with oxygen than Fe.[1–3] Those Cr oxide inclusions would float up into the liquid mold flux under the overall forces exerted by buoyancy, fluid flow, bubbles, etc.[4–6] Then, the performance of the mold flux will be deteriorated with the pickup of chromium oxides in the liquid slag, which, in turn, leads to the defects occurring on both the surface and interior of the final strand. Khater and Idris[7] investigated the effect of Cr_2O_3 on the melting temperature and crystallization of aluminosilicate glass and found that Cr_2O_3 tends to increase the melting temperature and enhance the crystallization of the glass. Marghussian and Arjomandnia[8] studied the crystallization behavior of glassy ceramics in the presence of Cr_2O_3 nucleates and suggested that the crystallization ability of glassy ceramics was improved. Similar results were also obtained by Bin Hussian et al.[9] and Barbieri et al.[10] Besides, Xu et al.[11] conducted research regarding the effect of Cr_2O_3 on the melting, viscosity, heat-transfer, and crystallization behaviors of mold flux used for the casting of Cr-bearing alloy steels and concluded that the melting temperature and viscosity of the mold flux were increased significantly, whereas the heat-transfer rate and crystallization ability were lowered, with the increase of Cr_2O_3 content.

Therefore, from the previous research, the property of mold flux is really varied with the absorption of chromium oxides inclusions. In order to compensate this negative effect during the continuous casting process, the composition of the mold flux was specially designed in this study, through adding effective fluxing agents, such as B_2O_3 and MnO, into the flux as well as adjusting its basicity (R). Then, the melting, viscosity, crystallization, and heat-transfer behaviors of those designed mold fluxes were investigated in this article.

II. EXPERIMENTAL METHOD

A. Experimental Materials Preparation

The compositions of designed mold fluxes in this study were adjusted based on a commercial benchmark mold flux sample 1 for casting Cr-contained steel,

WANLIN WANG, JIE YU, LEJUN ZHOU, and HUAN LI are with the School of Metallurgy and Environment, Central South University, Changsha 410083, P.R. China. Contact email: l.j.zhou@hotmail.com ZHAOYANG WU is with the Key Laboratory of Metallurgical Emission Reduction & Resources Recycling, Anhui University of Technology, Ma'anshan 243002, P.R. China.

through changing the content of B_2O_3, MnO, Cr_2O_3, and basicity, as shown in Table I. All samples were prepared first by melting reagent grade chemicals of $CaCO_3$, SiO_2, Al_2O_3, Na_2CO_3, CaF_2, $MnCO_3$, Cr_2O_3, and B_2O_3 in an induction furnace at 1773 K (1500 °C) for 5 minutes to homogenize their chemical compositions. Then, the samples for the heat-transfer tests were obtained by pouring the melts onto a steel plate; meanwhile, a new cylindrical tubelike copper mold with a diameter of 20 mm was used to cast the liquid mold flux before it solidified. After that, the cooled mold flux disks were polished by using SiC sandpapers with a grit size down to 1200 to control their surface roughness and thickness. The polished glassy samples were then placed on the top of the copper mold individually for heat-transfer experiments through the infrared emitter technique (IET).

The samples for the melting and crystallization tests were obtained through sampling a small amount of homogeneous molten mold flux and quenching it into glass. After that, the solidified glassy mold flux was crushed and ground into powder samples for the melting and crystallization tests through single hot thermocouple technique/double hot thermocouple technique (SHTT/DHTT) experiments. Besides, the samples for the viscosity measurement tests were prepared through stirring those reagent grade chemicals in a blender for 120 minutes. The premelted mold fluxes were also analyzed by X-ray fluoroscopy (S4 Pioneer, Bruker AXS, GmbH Karlsruhe, Germany), and the results are shown in Table I.

B. SHTT/DHTT Test

The melting temperature range of mold flux was measured by the SHTT test, whereas the crystallization behavior was characterized by the DHTT test. The schematic figures of SHTT/DHTT are shown in Figure 1.[12,13]

During the melting test, the mold flux sample powders were first mounted on a B-type thermocouple, as shown in Figure 1(b). Then, the thermocouple, together with the powders, was heated at a rate of 15 K (°C)/s. The variation of mold flux sample was observed and recorded through a CCD microscope connected to a DVD recorder. Meanwhile, the corresponding temperature history was obtained by the temperature acquisition system. Combining the *in-situ* video and variation of temperature history, the melting behavior of mold fluxes could be well investigated.

For the crystallization test, the slag sample powders were mounted between two B-type thermocouples (CH-1 and CH-2), as shown in Figure 1(c). A desired temperature gradient between the two thermocouples could be achieved through controlling the temperature of each thermocouple separately. During the crystallization test, the distance between the two thermocouples was set as 2 mm and the hot thermocouple (CH-1) was set as 1673 K (1400 °C) to simulate the shell surface temperature, whereas the cold thermocouple (CH-2) was used to simulate the solid mold flux interface temperature 1073 K (800 °C) according to the previous article.[14,15]

C. Viscometer Test

The viscosity measurements were carried out using a Brookfield DV-II+ viscometer (Brookfield Inc.) through the rotating cylinder method, and the equipment is schematically shown in Figure 2. A calibration measurement was carried out at room temperature using the stand oil with known viscosity.[16]

When measuring the viscosity of the mold fluxes, first, about 250 g of the sample powders were placed in a graphite crucible with diameter and internal height of 50 and 80 mm, respectively. Second, the crucible was heated to 1773 K (1500 °C) and held for 10 minutes to obtain a homogeneous melt in an electric resistance furnace with $MoSi_2$ as the heating element. Then, the melt was cooled to the target temperature. After that, a bob, which was made of molybdenum with 18-mm height and 15-mm diameter, was immersed into liquid slag bath and rotated to obtain the value of viscosity at the target temperature.

D. IET Test

The heat-transfer behaviors of mold flux were investigated by using the IET, which is schematically shown in Figure 3. The details of the IET have been described elsewhere.[17,18] The copper mold system was first heated under the incident thermal energy, increased linearly to 500 kW/m^2 and maintained for 300 seconds to preheat the slag disk. Then, the incident thermal energy was increased continuously to 800 kW/m^2 and maintained for another 300 seconds. After that, the incident heat flux was further increased to 1400 kW/m^2, which is in the magnitude of the real caster, and maintained for 400 seconds. The heat flux across the mold flux disk was calculated through the one-dimensional inverse heat conduction model developed by Beck,[19] based on the measured temperature from the embedded thermocouples. As the thermal properties are functions of temperature and time, the one-dimensional inverse heat conduction is sufficient to use with only one internal body temperature and one boundary condition to

Table I.   Chemical Composition of Mold Fluxes after Premelting (Weight Percent)

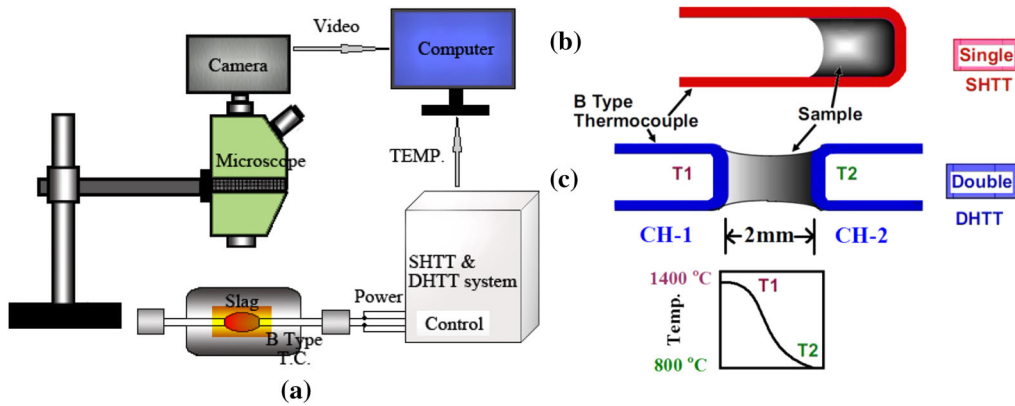| Flux	SiO_2	CaO	Al_2O_3	Na_2O	F	MnO	Cr_2O_3	B_2O_3	R
1	33.88	32.71	3.72	14.25	12.74	0	0	0	0.96
2	32.35	31.13	3.68	14.24	12.72	1.11	2.12	0	0.96
3	30.79	29.66	3.71	14.22	12.71	1.12	2.12	3.00	0.96
4	29.37	30.92	3.62	14.29	12.81	1.11	2.11	3.01	1.05
5	27.99	32.19	3.61	14.35	12.84	1.10	2.10	3.01	1.15

Fig. 1—Schematic configuration of SHTT/DHTT: (a) schematic of experimental apparatus, (b) SHTT, and (c) DHTT.
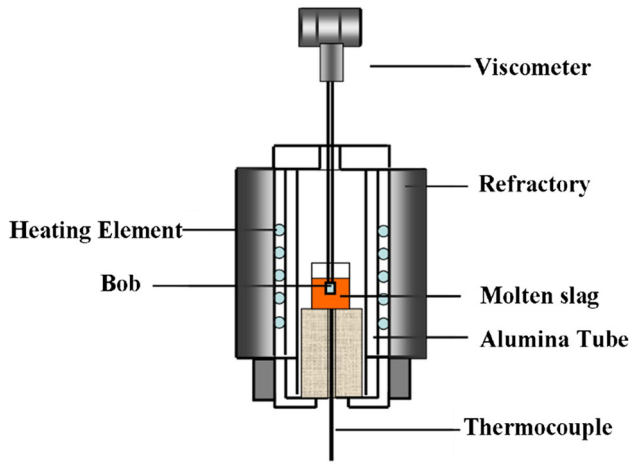

Fig. 2—Schematic figure of the viscometer.

determine the unknown boundary condition and to estimate the heat flux by using the measured transient interior temperature through Eq. [1]:

$$\frac{\partial}{\partial x}\left(k\frac{\partial T_i}{\partial x}\right) = (\rho c_p)\frac{\partial T_i}{\partial t} \quad [1]$$

where x is the distance below the top surface, k is the thermal conductivity, T is the temperature, ρ is the mass density of copper, t is the time, and c_p is the copper heat capacity.

The slag disks after the IET tests were crushed and ground into powder samples for X-ray diffraction (XRD) analysis. The crystalline phase composition was then detected by an X-ray diffractometer (RIGAKU-TTR III, Rigaku Corporation) with Cu K_α (0.154 184 nm). The XRD data were collected in a range of 2θ = 10 to 80 deg with a step size of 10 deg/min.

III. RESULTS AND DISCUSSION

A. Melting Behaviors

The responding temperature history and the snapshots for typical stages during the melting test process of the benchmark flux 1 are shown in Figure 4. At the very beginning, flux 1 is kept in a solid state due to the low heating temperature. Then, the powders start to sinter when the temperature reaches 993 K (720 °C). When the temperature approaches 1148 K (875 °C), flux 1 starts to melt, and it is completely melted at the temperature of 1340 K (1067 °C). It can be seen in Figure 4 that there is a temperature deviation appearing in the curves during the melting process. Before the initial melting of the powder mold fluxes, the temperature increases linearly with a heat rate of 15 K (°C)/s. Then, the temperature gradually deviates from the preset heating rate line when the melting process initiates due to the endothermic reaction of the melting process. The temperature would then increase linearly again when the melting process completes. These temperature deviations would last for a period called the "melting temperature range."

In order to compare the melting behavior of the benchmark flux 1 with the other four designed fluxes 2 through 5, the initial and complete melting temperature are shown in Figure 5. It can be found that the melting temperature ranges of both the benchmark and designed mold fluxes are close, ranging from [1124 K to 1395 K (851 °C to 1122 °C)]. More specifically, the initial/complete melting temperature increases from flux 1 [1148 K/ 1340 K (875 °C/1067 °C)] to flux 2 [1154 K/1384 K (881 °C/1111 °C)] with the addition of 1.1 pct MnO and 2.1 pct Cr_2O_3. Although MnO can work as a fluxing agent in the mold flux system, the melting temperature range still increases as Cr_2O_3 is a high melting oxide with melting temperature of 2538 K (2265 °C).[20] The initial/complete melting temperature then decreases for flux 3 [1124 K/1352 K (851 °C/1079 °C)] when 3.0 pct B_2O_3 is added, whereas it increases for flux 4 [1135 K/ 1392 K (862 °C/1119 °C)] and flux 5 [1143 K/1395 K (870 °C/1122 °C)] when the basicity is improved to 1.05 and 1.15. It is because B_2O_3 is a typical fluxing agent,[21,22] which can lower the melting temperature range of mold flux effectively. When the basicity increases in fluxes 4 and 5, it means the amount of CaO is added and then the melting temperature range is getting higher.

A comprehensive comparison of the initial and complete melting temperatures, as well as the melting

temperature range of fluxes 1 through 5, suggests that the designed fluxes 3 and 5 have the closest melting behavior to the benchmark flux 1.

B. *Viscosity*

The log η *vs* $1/T$ values of fluxes 1 through 5 are shown in Figure 6. First, it can be seen from Figure 6 that the viscosity of mold flux increases slowly with the decrease of temperature at the high-temperature zone, whereas it starts to increase sharply when the temperature reaches a certain value, which is called the "break temperature" according to Mills.[23] The break temperature is usually considered a key benchmark to indicate that the mold flux begins to lose flow ability. The break temperatures of fluxes 1 through 5 are listed in Table II. They are 1302 K (1029 °C), 1330 K (1057 °C), 1224 K (951 °C), 1246 K (973 °C), and 1268 K (995 °C) for fluxes 1, 2, 3, 4, and 5, respectively. Besides, the viscosities at the temperature of 1573 K (1300 °C) for the preceding fluxes are also listed in Table II, as the 1573 K (1300 °C) is considered to be the average temperature of the liquid slag layer in the casting mold, where the viscosity for each sample is 0.07, 0.15, 0.06, 0.06, and 0.04 Pa s, individually.

Through comparing the viscosity at the temperature of 1573 K (1300 °C) and the break temperature of fluxes 1 and 2, it can be found that both increase from 0.07 to 0.15 Pa s and from [1302 K (1029 °C) to 1330 K (1057 °C)] with the addition of 1.1 pct MnO and 2.1 pct Cr_2O_3. This mainly results from the fact that Cr_2O_3 is expected to behave like Al_2O_3 to increase the viscosity of the mold flux as a network former according to a previous study.[11] However, the viscosity and break temperature of flux 3 decrease to 0.06 Pa s and 1224 K (951 °C) with the addition of 3 pct B_2O_3, as B_2O_3 can lower the melting temperature of mold flux and enhance the driving force to overcome the transportation energy barrier. The break temperature increases continuously from 1224 K (951 °C) for flux 3, to 1246 K (973 °C) for flux 4, then to 1268 K (995 °C) for flux 5, whereas the viscosity decreases from 0.06 to 0.04 Pa s with the increase of basicity, which may be due to the fact that the increase of basicity can offer more CaO working as a network breaker in the molten silicate structure system and breaks the bonds of Si-O-Si into Si-O; consequently, the silicate structure is simplified and the viscosity of molten mold flux at 1573 K (1300 °C) is also lowered.[24] However, the increase of basicity can also improve the crystallization ability of mold flux, which made the crystals precipitate at higher temperature, and then the break temperature increased. Therefore, based on the break temperature and the viscosity at 1573 K (1300 °C), it can be found that flux 5 shows the most similar rheological behavior to benchmark flux 1.

C. *Crystallization*

Figure 7 shows the temperature history and crystallization evaluation process of flux 1 during the DHTT test, in which it can be divided into four typical stages. During stage I, the mold flux sample is liquid, as the

temperature of both thermocouples is 1673 K (1400 °C). When the CH-2 cools to 1073 K (800 °C) in stage II, the glassy phase is formed in the vicinity of CH-2 due to the high cooling rate of 30 K/s. When the time reaches 317 seconds in stage III, the crystals are precipitated in the middle of the sample. The crystalline layer keeps growing toward both the high-temperature CH-1 and low-temperature CH-2, and then the final three layers (liquid, crystalline, and glassy) reach steady state in stage IV. The final distribution of the three layers reflects the general crystallization ability of mold flux.

The SEM of the mold flux samples after DHTT tests is shown in Figure 8. There are glassy and crystalline phases formed in the samples, among which glass 1 in the left side of the samples is formed through the direct cooling of the residual liquid mold flux in the vicinity of high-temperature CH-1, as its shape is circular due to the solidification shrinkage after the DHTT test. Glass 2 in the right is the original one that precipitated during stage 2, as the fracture is uneven. Between them, crystals are precipitated. In order to evaluate the crystallization ability of the benchmark and newly designed mold fluxes, the fractions of each phase in fluxes 1 through 5 after the DHTT tests are listed in Figure 9.

It can be seen from Figure 9 that the crystalline fraction decreases from 81.0 pct (flux 1) to 42.1 pct (flux 2), then to 25.3 pct (flux 3), with the addition of MnO, Cr_2O_3, and B_2O_3 in the designed mold flux system. However, the crystalline fraction increases from 54.4 pct (flux 4) to 81.5 pct (flux 5) with the increase of basicity. The preceding phenomena can be explained as both Cr_2O_3 and B_2O_3 working as network formers, whereas CaO works as a network breaker in the molten silicate, as discussed in Section III–B. These network formers make the silicate structure more complex and introduce a higher polymerization degree, which can inhibit the crystallization process. Conversely, the increase of network breaker CaO simplifies the molecular/ions clusters and enhances the crystallization ability of the mold flux. Therefore, from the results of DHTT and SEM analyses, it can be obtained that flux 5 has the closest crystallization ability with the benchmark flux 1.

D. *Heat-Transfer Behaviors*

The measured heat flux and snapshots of typical stages during the IET test for flux 1 are shown in Figure 10. From stage i to stage iv, the slag disk remains glass, as the incident radiant heat from the IET is small and the responding temperature of the slag disk is low. However, the crystalline layer is observed to initiate on the top of the slag disk (the snapshot at 1200 seconds); meanwhile, the slope of the measured heat flux decreases compared with the slopes in stages i and iii at the time before 1423 seconds in stage v. The decrease of slope on the measured heat flux is caused by the formation of opaque crystals on the top of the disk, as the crystalline layer could reduce the heat flux across the disk due to the more reflected and scattered incident radiation by the crystal surface, grain boundary, and defects, which leads to less energy being absorbed and conducted to the mold.[25,26] However, the slope increases again later than
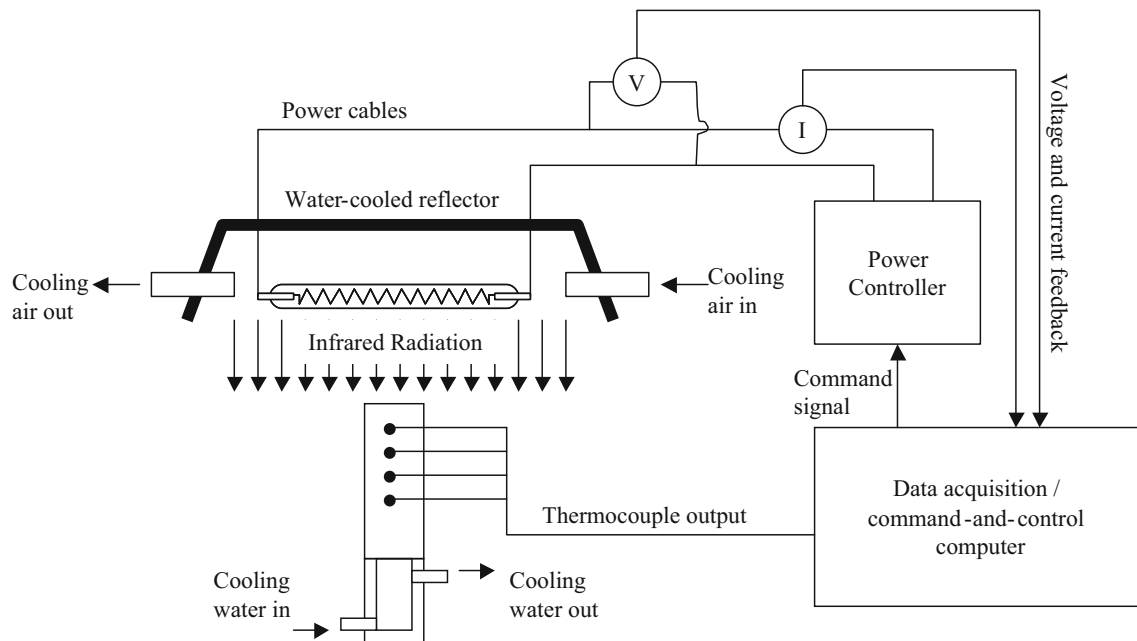
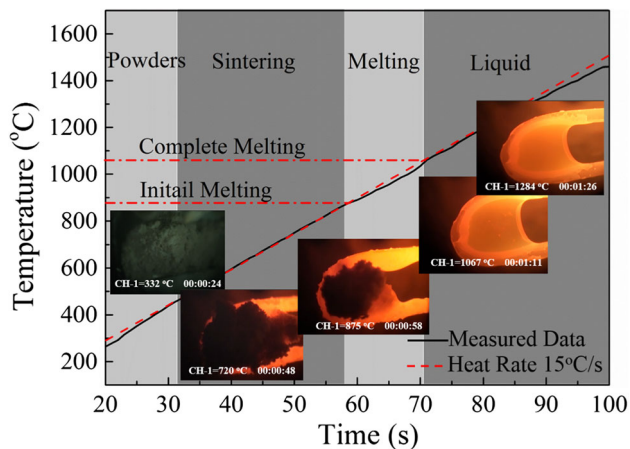Fig. 3—Schematic illustration of the infrared emitter.
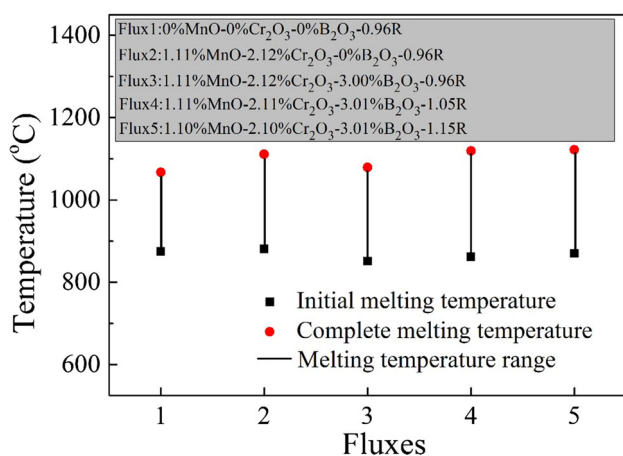

Fig. 4—Melting behavior of flux 1.

Fig. 5—Melting temperature of fluxes 1 through 5.

1423 seconds in stage v; meanwhile, the top part of the slag disk gets melted as it becomes arc shaped (the snapshot at 1500 seconds). The melted top part of the disk is beneficial for the enhancement of incident radiation heat, so the slope of the measured heat flux increases. Finally, the heat flux steps into a steady state when the evolution of flux film structure (liquid, crystalline, and glass layers) becomes stable and the heat flux remains relatively constant, as shown in stage vi in Figure 10.

The measured heat fluxes for fluxes 1 through 5 in the final stage are combined in Figure 11, and it can be found that the final measured heat flux increases from 695.9 MW/m^2 (flux 1), to 756.7 MW/m^2 (flux 2), then to 784.5 MW/m^2 (flux 3) with the addition of MnO, Cr$_2$O$_3$, and B$_2$O$_3$, whereas it decreases from 712.2 MW/m^2 (flux 4) to 672.8 MW/m^2 (flux 5) with the improvement of basicity. Comparing the tendency of the measured heat flux and crystallization ability of mold fluxes suggests that the influences of these oxides are different. In fact, the tendency is mainly due to the heat-transfer ability of the mold flux being directly determined by its crystallization capability, which is determined by the composition of the mold flux itself.

The XRD patterns of benchmark flux 1 and designed fluxes 2 through 5 after the IET tests are shown in Figure 12, in which the main characteristic peaks of all mold fluxes are similar to each other, suggesting that the main crystals precipitated in mold fluxes are cuspidine (Ca$_4$Si$_2$O$_7$F$_2$). Besides, the intensity of these characteristic peaks also indicates that the crystallization ratio of mold flux decreases from flux 1 to flux 2, then to flux 3, whereas it increases from flux 4 to flux 5, which is consistent with the results of DHTT and IET tests. Therefore, the results of IET tests imply that flux 5 has

Table II.   Viscosity at 1573 K (1300 °C) and Break Temperature of Fluxes 1 through 5

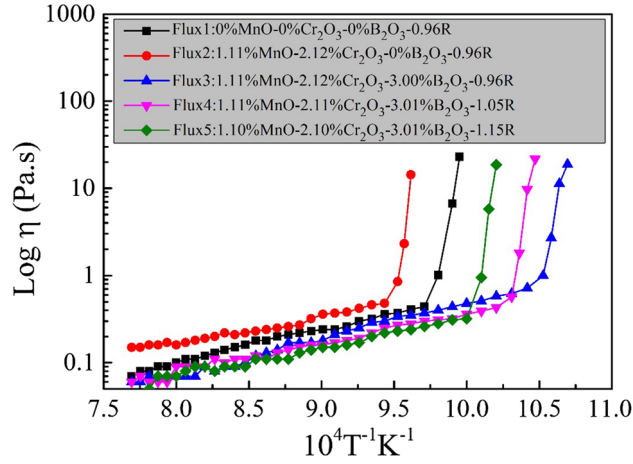| Flux	1	2	3	4	5
T_{br} (°C)	1029	1057	951	973	995
Viscosity (Pa s)	0.07	0.15	0.06	0.06	0.04

Fig. 6—Viscosity-temperature curve of fluxes 1 through 5.
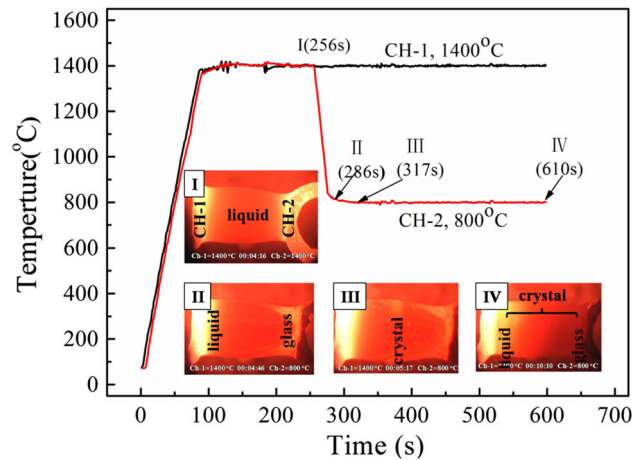
Fig. 7—Crystallization evolution process of flux 1.

Fig. 8—SEM photos for the samples after DHTT experiment: (a) flux 1, (b) flux 2, (c) flux 3, (d) flux 4, and (e) flux 5.

the most similar heat-transfer behavior to the benchmark mold flux.

IV.   CONCLUSIONS

The melting, viscosity, heat-transfer, and crystallization behaviors of benchmark and newly designed mold fluxes for casting Cr-contained steel have been investigated by SHTT/DHTT, viscometer, and IET systematically, and the specific conclusions are summarized as follows.

1. The melting temperature range for the newly designed mold fluxes is from [1124 K to 1395 K (851 °C to 1122 °C)], and it is close to the benchmark mold flux that is from [1148 K to 1340 K (875 °C to 1067 °C)].
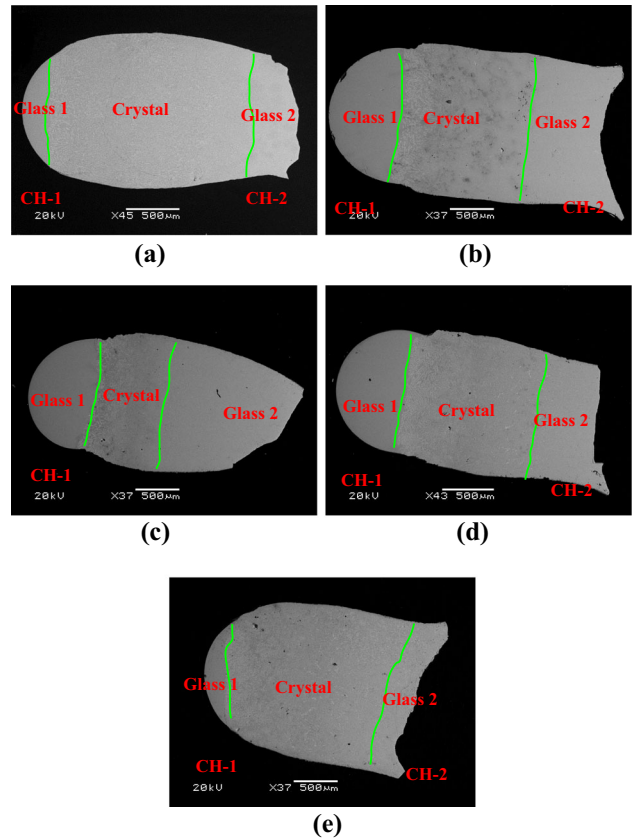
2. The viscosity at the temperature of 1573 K (1300 °C) and the break temperature increase from 0.07 to 0.15 Pa s and from [1302 K to 1330 K (1029 °C to 1057 °C)], respectively, with the addition of 1.1 pct MnO and 2.1 pct Cr_2O_3. However, they decrease to 0.06 Pa s and 1224 K (951 °C) with the addition of 3 pct B_2O_3. Then, the break temperature increases continuously from [1224 K to 1246 K (951 °C to 973 °C)], and then to 1268 K (995 °C), whereas the viscosity reduces from 0.06 to 0.04 Pa s with the increase of basicity.

3. The crystalline fraction decreases from 81 to 42.1 pct, and then to 25.3 pct, with the addition of MnO, Cr_2O_3, and B_2O_3. However, it increases from 54.4 to 81.5 pct with the addition of basicity.

4. The influence of oxides on the heat-transfer behavior of mold fluxes is opposite to the role they have played for the mold flux crystallization, as the heat-transfer ability of mold flux is directly determined by its
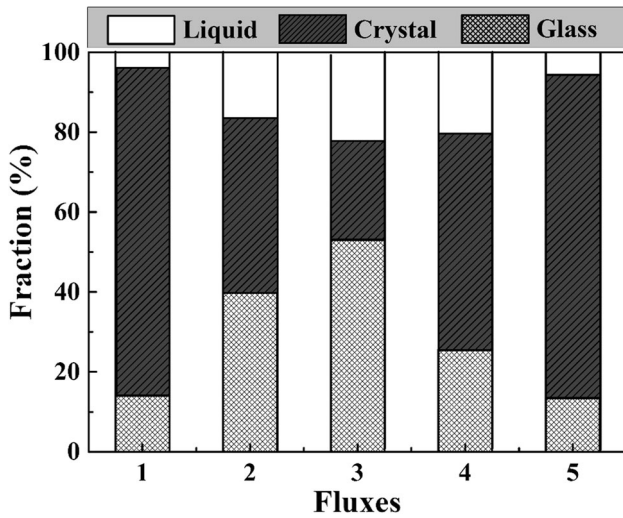
Fig. 9—Fraction of each phase distribution in the samples after DHTT experiments.
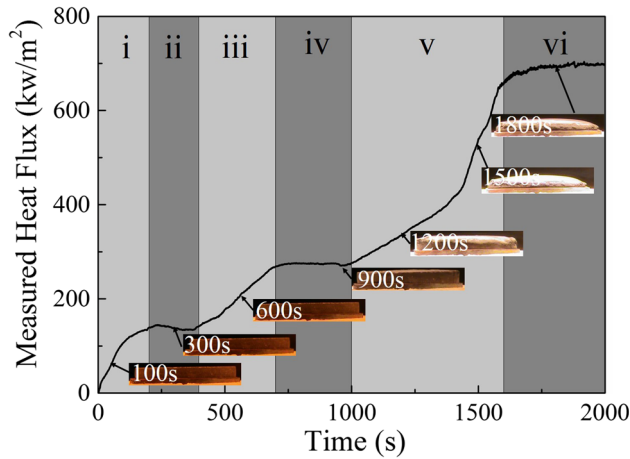

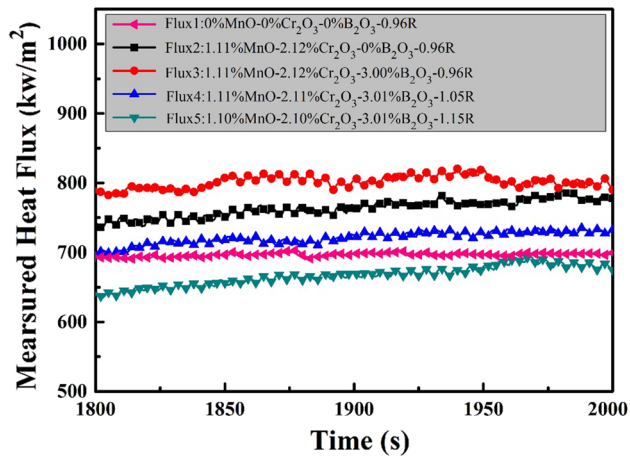Fig. 10—Measured heat flux history of flux 1.

Fig. 11—Final state measured heat flux histories for fluxes 1 through 5.
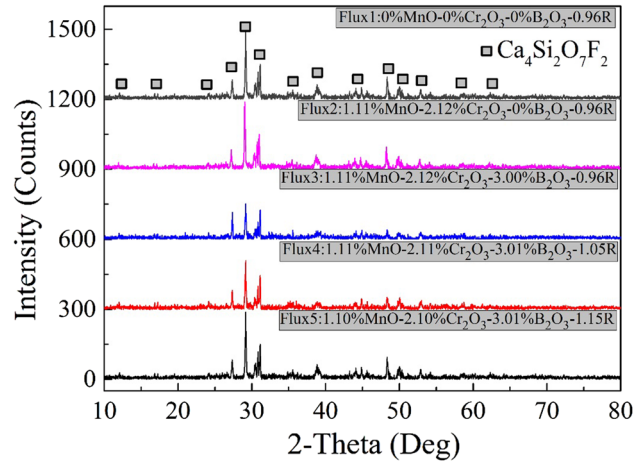

Fig. 12—XRD pattern of the mold fluxes 1 through 5.

crystallization capability, which depends on the major composition of the mold flux itself.

5. Comprehensive comparison of the melting, viscosity, heat-transfer, and crystallization behaviors of the four designed mold fluxes suggests that flux 5 shows the most similar properties as the benchmark commercial flux 1.

REFERENCES

1. P. Yan, S. Huang, L. Pandelaers, J.V. Dyck, M. Guo., and B. Blanpain: *Metall. Mater. Trans. B*, 2013, vol. 44B, pp. 1105–19.
2. T. Nakasuga, K. Nakashima, and K. Mori: *ISIJ Int.*, 2004, vol. 44, pp. 665–72.
3. Y. Okabe, I. Tajima, and K. Ito: *Metall. Mater. Trans. B*, 1998, vol. 19B, pp. 131–36.
4. L. Zhang: *JOM*, 2012, vol. 64, pp. 1059–62.
5. B.G. Thomas, Q. Yuan, S. Mahmood, R. Liu, and R. Chaudhary: *Metall. Mater. Trans. B*, 2014, vol. 45B, pp. 22–35.
6. H. Arai, K. Matsumoto, S. Shimasaki, and S. Taniguchi: *ISIJ Int.*, 2009, vol. 49, pp. 965–74.
7. G.A. Khater and M.H. Idris: *Ceram. Int.*, 2009, vol. 35, pp. 69–75.
8. V.K. Marghussian and S. Arjomandnia: *Phys. Chem. Glasses*, 1999, vol. 40, pp. 311–13.
9. M.A. Bin Hussain, M.H. Idrees, and M.M. Khan: *J. Therm. Anal. Calorim.*, 2002, vol. 67, pp. 563–77.
10. L. Barbieri, C. Leonelli, T. Manfredini, G.C. Pellacani, G.C. Pellacani, E. Tondello, and R. Bertoncello: *J. Mater. Sci.*, 1994, vol. 29, pp. 6273–80.
11. C. Xu, W. Wang, L. Zhou, S. Xie, and C. Zhang: *Metall. Mater. Trans. B*, 2015, vol. 46B, pp. 882–92.
12. L. Zhou, W. Wang, F. Ma, J. Li, J. Wei, H. Matsuura, and F. Tsukihashi: *Metall. Mater. Trans. B*, 2012, vol. 43B, pp. 354–62.
13. W. Wang, X. Yan, L. Zhou, S. Xie, and D. Huang: *Metall. Mater. Trans. B*, 2016, vol. 47B, pp. 963–73.
14. L. Zhou, W. Wang, D. Huang, J. Wei, and J. Li: *Metall. Mater. Trans. B*, 2012, vol. 43B, pp. 925–36.

15. L. Zhou, W. Wang, R. Liu, and B.G. Thomas: *Metall. Mater. Trans. B*, 2013, vol. 44B, pp. 1264–79.
16. L. Zhou, W. Wang, and K. Zhou: *Metals*, 2016, vol. 6, pp. 139–53.
17. W. Wang and A.W. Cramb: *ISIJ Int.*, 2005, vol. 45, pp. 1864–70.
18. W. Wang, K. Blazek, and A. Cramb: *Metall. Mater. Trans. B*, 2008, vol. 39B, pp. 66–74.
19. J.V. Beck: *1HCP1D: Version* 5.31, Beck Engineering Consultants Company, Houston, TX, 1997.
20. A. Muan and S. Omiya: *J. Am. Ceram. Soc.*, 1960, vol. 43, pp. 204–09.
21. A.B. Fox, M.E. Valdez, J. Gisby, R.C. Atwood, P.D. Lee, and S. Sridhar: *ISIJ Int.*, 2004, vol. 44, pp. 836–45.
22. H. Kim and I. Sohn: *ISIJ Int.*, 2011, vol. 51, pp. 1–8.
23. K.C. Mills, A.B. Fox, Z. Li, and R.P. Thackray: *Ironmak. Steelmak.*, 2005, vol. 32, pp. 26–34.
24. G. Kim, C. Kim, and I. Sohn: *ISIJ Int.*, 2013, vol. 53, pp. 170–76.
25. S. Ozawa, M. Susa, T. Goto, R. Endo, and K.C. Mills: *ISIJ Int.*, 2006, vol. 46, pp. 413–19.
26. J. Cho, H. Shibata, T. Emi, and M. Suzuki: *ISIJ Int.*, 1998, vol. 38, pp. 834–42.